Spectrochimica Acta Part A: Molecular and Biomolecular Spectroscopy 311 (2024) 123974

Contents lists available at ScienceDirect

Spectrochimica Acta Part A: Molecular and Biomolecular Spectroscopy

journal homepage: www.journals.elsevier.com/spectrochimica-acta-part-a-molecular-and-biomolecular-spectroscopy

Colloidal surface-enhanced Raman spectroscopic study of grouper epidermal mucus using acidified sodium sulphate as the aggregating agent

Nathaniel Leong [a], Mohd Hanif Yaacob [a], Ahmad Rifqi Md Zain [b], Tengku Hasnan Tengku Abdul Aziz [b], Annie Christianus [c], Chou Min Chong [c,d], Mohd Adzir Mahdi [a,e,*]

[a] Wireless and Photonics Networks Research Centre, Faculty of Engineering, Universiti Putra Malaysia, 43400 Serdang, Selangor, Malaysia
[b] Institute of Microengineering and Nanoelectronics (IMEN), Universiti Kebangsaan Malaysia, 43600 Bangi, Selangor, Malaysia
[c] Department of Aquaculture, Faculty of Agriculture, Universiti Putra Malaysia, 43400 Serdang, Selangor, Malaysia
[d] Laboratory of Sustainable Aquaculture (AquaLab), International Institute of Aquaculture and Aquatic Sciences (I-AQUAS), Universiti Putra Malaysia, 71050 Port Dickson, Negeri Sembilan, Malaysia
[e] Institute of Nanoscience and Nanotechnology (ION2), Universiti Putra Malaysia, 43400 Serdang, Selangor, Malaysia

HIGHLIGHTS

- Acidified sodium sulphate was used as the aggregating agent for colloidal SERS.
- Enhancement of SERS signal from the analytes; rhodamine 6G, lysozyme and mucus.
- Overlapping peaks in the SERS spectrum of lysozyme and grouper mucus were observed.
- Lysozyme can be possibly detected in grouper epidermal mucus using SERS analysis.

GRAPHICAL ABSTRACT

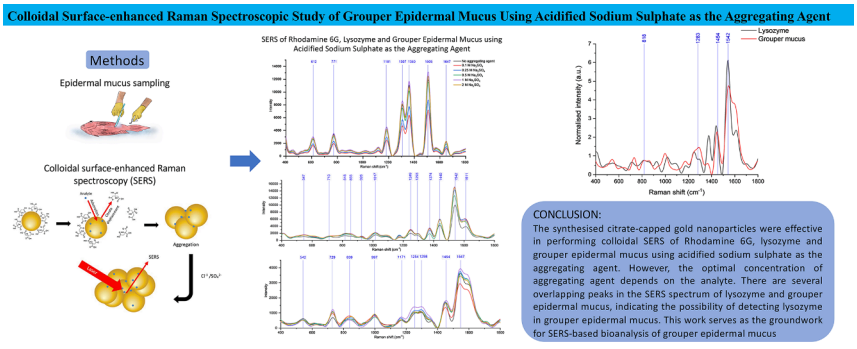

ARTICLE INFO

Keywords:
Fish epidermal mucus
Surface-enhanced Raman Spectroscopy
Aggregating agent
Lysozyme
Gold nanoparticles

ABSTRACT

Fish epidermal mucus is an important reservoir of antipathogenic compounds which serves as the first line of the immune defence. Despite its significant role in the physiology and health of fish, detailed profiling of fish epidermal mucus has yet to be explored. Therefore, this study investigates a label-free colloidal surface-enhanced Raman spectroscopic (SERS) method for profiling grouper mucus. Gold nanoparticles were first synthesised using the standard citrate reduction and characterised using ultraviolet–visible spectroscopy, transmission electron microscopy and dynamic light scattering. The influence of acidified sodium sulphate (Na_2SO_4) at pH 3 as the aggregating agent on the enhancement of the SERS spectrum of different analyte samples including rhodamine 6G (R6G) dye, lysozyme solution and hybrid grouper (*Epinephelus fuscoguttatus* × *Epinephelus lanceolatus*) mucus was observed. Based on the results, an optimal Na_2SO_4 concentration of 1 M was recorded to achieve the highest enhancement of the SERS signal for R6G and grouper mucus, while the optimal concentration for lysozyme was 0.1 M. The results indicated a higher degree of aggregation induced by lysozyme than R6G and grouper mucus. A

* Corresponding author.
E-mail address: mam@upm.edu.my (M.A. Mahdi).

https://doi.org/10.1016/j.saa.2024.123974
Received 13 October 2023; Received in revised form 24 January 2024; Accepted 27 January 2024
Available online 1 February 2024

few overlapping peaks of the SERS spectra of lysozyme and grouper mucus made it possible to confirm the presence of lysozyme as potential biomarkers.

1. Introduction

Fish epidermal mucus is constantly in contact with the marine environment, making it a vital first line of defence against pathogens. The mucus is continually secreted by the goblet cells, sacciform cells and club cells in the epidermis throughout the body [1]. Interestingly, the epidermal mucus is rich in antimicrobial compounds, including lysozyme, lectins and proteases, that provide innate immunity against numerous pathogenic species [2]. Although fish mucus profiling offers valuable insight into the physiology and health of fish, certain drawbacks such as the necessity for rapid processing to avoid the breakdown of mucus components, issues in identifying and quantifying compounds in low concentration, difficulties in characterising complex compounds, and lack of standardised protocols for collection, preparation, and analysis could result in inconsistent findings between studies [3].

Surface-enhanced Raman spectroscopy (SERS) has become a reliable technique due to its rapid and sensitive nature in characterising samples prone to rapid degradation. SERS depends on the adsorption of analyte molecules on plasmonic nanostructures, where the Raman scattering of the target molecule is enhanced many times, up to 10^6 orders of magnitude [4]. The Raman reporter or label-free method is typically employed to target analyte biomolecules. On the one hand, Raman reporters involve functionalising the surface of nanoparticles with specific dye molecules and other ligands such as antibodies or oligonucleotides. Subsequently, the signal from the dye molecule is measured to indicate a binding event between the target molecule and ligand on the nanoparticle surface [5]. On the other hand, the label-free method detects the signal biomolecules directly adsorbed on the nanoparticle surface. Despite the ability of the latter to directly analyse the target biomolecules, some biomolecules exhibit a low scattering cross-section, making it difficult to obtain a reliable outcome [6].

The application of label-free SERS of biofluid in biological analysis, particularly in the field of disease diagnosis has been explored by many researchers. Typically, the SERS spectra of biofluid are analysed using a combination of principal component analysis (PCA) and linear discriminant analysis (LDA). PCA reduces the dimensionality of the spectral data to a few principal components which are used for the classification of patient's health status using LDA, that determines a linear boundary between the healthy and unhealthy patients [7]. For example, SERS of biofluid coupled with PCA and LDA has been demonstrated to diagnose Sjörgen's syndrome using patient's saliva samples [8] and prostate cancer from patient's urine sample [9]. Additionally, this method has been applied in the classification of the severity of knee osteoarthritis [10] and the classification of the histological grade of oral squamous cell carcinoma using serum samples [11].

The electrostatic interaction between the analyte molecules and the surface charge of the metallic nanoparticles greatly influences SERS analysis in the colloidal system. Optimal scattering efficiency is enhanced when the analyte molecules are trapped in the nanogaps between the nanoparticles, forming the SERS hot spots [12]. Therefore, controlling the aggregation of the nanoparticles is key to obtaining the best SERS signal. As such, the use of the colloidal system makes it possible to study fish epidermal mucus in its native form without the need of drying, as opposed to SERS substrates fabricated using immobilised metallic nanostructures on a solid substrate [13,14].

In view of this, the label-free SERS method is the most straightforward and cost-efficient method for exploring fish epidermal mucus. However, to the best of the author's knowledge, no study has examined fish epidermal mucus using SERS so far. Besides the scarce information on disease markers in fish epidermal mucus, there is a limited supply of off-the-shelf ligands that bind with the biomolecules in fish epidermal mucus. Concurrently, it is costly and time-consuming to sequence these ligands (antibodies or oligonucleotides) for surface functionalisation of the plasmonic nanoparticles.

There are a few published research works on the colloidal SERS of human biofluids using several types of aggregating agents. For example, SERS analysis of human serum and urine samples were conducted using silver nanoparticles and calcium nitrate as the aggregating agent [15]. In another work, propranolol was detected in human plasma, serum and urine using SERS analysis facilitated by silver nanoparticles and sodium chloride as the aggregating agent [16]. Acidified sodium sulphate (Na_2SO_4) solution at pH 3 was shown to be an effective aggregating agent for detecting low protein concentrations [6]. Therefore, this study addresses the gap in research for an optimised protocol for SERS analysis of grouper epidermal mucus and proposes an optimised label-free SERS protocol using acidified Na_2SO_4 as an aggregating agent to obtain the best signal enhancement from grouper epidermal mucus.

2. Materials and methods

2.1. Materials and reagents

Gold (III) chloride solution ($HAuCl_4$, 99.99 % trace metal basis, 30 % wt in diluted hydrochloric), sodium citrate dihydrate (Na_3Ct, USP testing specifications), sodium sulphate (Na_2SO_4, ACS reagent grade), lysozyme from hen egg white and rhodamine 6G (R6G, 99 % pure) were purchased from Sigma-Aldrich. All syntheses were carried out in deionised water. An appropriate amount of Na_2SO_4 was dissolved in deionised water to achieve a series of concentration of 2, 1, 0.5, 0.25 and 0.1 M. The final pH level of the aggregating agents was adjusted to pH 3 using 1 % sulphuric acid (H_2SO_4) solution. Similarly, 300 μg/mL and 1 mM of lysozyme and R6G solutions were prepared by mixing an appropriate amount of lysozyme and R6G solution in deionised water, respectively.

2.2. Instrumentation

The characterisation of the gold nanoparticles was performed using ultraviolet–visible spectroscopy (UV–Vis, Lambda 35, Perkin Elmer), dynamic light scattering (DLS, Zetasizer Nano-S, 633 nm, Malvern Panalytical) and transmission electron microscopy (TEM, JEOL JEM 2100F Field Emission TEM). In addition, the Raman spectroscopy setup consisted of a 785 nm narrow linewidth source (XIM-6206–785-500–2, Yixi Intelligent Technology), high sensitivity spectrometer (YIM-6703-01-S03L01F05G02, Yixi Intelligent Technology), a 785 nm Raman probe (Wasatch Photonics) and a Raman immersion probe with a sapphire ball lens (MarqMetrix). To analyse the detected signals, baseline correction and spectral pre-processing were performed using OriginLab Pro (ver. 2018, OriginLab Corporation).

2.3. Synthesis and characterisation of gold nanoparticles

Gold nanoparticles were synthesised using the standard citrate reduction proposed by Turkevich et al. [17] with some modifications. Approximately, 50 mL of 0.25 mM $HAuCl_4$ solution (pH ~ 3) was prepared in an Erlenmeyer flask. The solution was placed on a hotplate, stirred rapidly at 500 rpm and heated until boiling at 100 °C. Once the solution reached its boiling point, 367.6 μL of 38.25 mM Na_3Ct solution (1.12 M ratio for $HAuCl_4$ to Na_3Ct) was injected into the solution. The mixture was continuously stirred at 100 °C for an hour. The flask was covered with aluminium foil with a beaker of ice placed on top to minimise solvent loss by condensing the steam. The heat was turned off

after an hour and the gold colloid was left to cool to room temperature while constantly stirred. Deionised water was added to the cooled colloid up to a final volume of 50 mL. Finally, the colloid was then stored in a brown bottle in the refrigerator at 4 °C until further analysis.

2.4. Characterisation of gold nanoparticles

The absorption spectra of the gold colloid were analysed using UV–vis spectroscopy [18], while the diameter of the gold nanoparticles was determined using TEM [19]. Approximately 10 μL of the colloid was dropped and dried on a copper mesh grid for TEM imaging. Additionally, the particle size and polydispersity of the gold nanoparticles were measured using DLS in triplicate measurements [20]. The gold colloid was diluted five times using deionised water for UV–vis spectroscopy and DLS analysis.

2.5. Mucus sampling

Three 25-litre aquariums were initially cleansed and filled with 10 L of saltwater. These three aquariums were namely as the holding aquarium, anaesthetising aquarium and recovery aquarium. The anaesthetising aquarium was added with 100 ppm tricaine methanesulfonate to anaesthetise the fish [21] for easier handling during mucus collection. Five groupers (length ~ 15 cm) were transferred to the holding aquarium from the main tank. Silicon scrappers were then sanitised with 70 % (v/v) isopropanol before scraping the mucus into a microcentrifuge tube. Next, one of the fishes was transferred from the holding aquarium and left in the anaesthetising aquarium for a few minutes until the fish showed minimal movements. Subsequently, the epidermal mucus was collected by scarping the mucus from the fish body from head to tail on both sides using the silicon scrappers into a 1.5 mL microcentrifuge tube. After collecting the mucus, the fish was placed into the recovery aquarium for the anaesthesia to wear off before returning to the main tank. Next, scales and impurities were carefully removed from the mucus samples. The collected mucus samples were then pooled together and homogenised by briefly sonicating the mucus with an ultrasonicator probe. The homogenised mucus was divided into aliquots of 100 μL each in a microcentrifuge tube and stored in a freezer at −20 °C until further analysis.

2.6. Sample preparation

The sample preparation method by Turzhitsky et al. [12] was used for Raman measurement with minor adjustments. Prior to SERS analysis, excess citrate and unreacted reactants were removed from the gold nanoparticles by centrifuging at 4000 rpm for 30 min and redispersed in deionised water. After the washing process was carried out for three cycles, the gold colloid recorded a pH level of ~ 7. Next, approximately 4.5 mL of the gold colloid was centrifuged at 4000 rpm and 30 min, and then removing an appropriate amount of the supernatant to achieve a final volume of 50 μL. Subsequently, 9.5 μL of the gold nanoparticles were mixed with 10 μL of the analyte solution, followed by 0.5 μL of the aggregating agent or deionised water (for control). Instead of relying on the random Brownian motion of the molecules to form the aggregates, the mixture was vortexed at 1000 rpm for 1 min to introduce forced convection to promote a more uniform formation of aggregates [22]. The mixture was incubated for another minute before being transferred to a concave glass slide wrapped with aluminium foil for the SERS analysis.

2.7. Raman measurement

The immersion probe method was used for the Raman measurement, in which the liquid droplet was brought in contact with the ball lens of the immersion probe (see Figure S1 in the supplementary material). In this method, uncertainties caused by the position of the beam waist within the liquid droplet, which depends on the geometry of the liquid droplet were removed. The laser power (measured at the output fibre ferrule) was 50 mW for R6G and 150 mW for lysozyme and grouper mucus with an integration time of 10 s. It was necessary to use a lower laser power for R6G to avoid the detector's saturation effect. The spectra were smoothed using the Savitzky-Golay algorithm with a 13-point window and cubic polynomial to remove shot noises. These parameters were applied given their ability to produce an ideal signal-to-noise ratio and maintain most spectral characteristics [23]. A baseline correction was performed using the asymmetric least square smoothing algorithm in OriginLab Pro (asymmetric factor of 0.001, threshold of 0.1, smoothing factor of 4, and 10 iterations). The spectra were smoothed again using the Savitzky-Golay algorithm with the same parameters to further denoise the spectra before being subjected to a constant subtraction to set the baseline at zero.

3. Results and discussion

3.1. Characterisation of gold nanoparticles

Fig. 1(a) shows the absorbance peak of the gold nanoparticles was recorded at 537 nm wavelength. Haiss et al. determined that the relationship between the wavelength of the absorbance peak (λ_{abs}) and the diameter of gold nanoparticles, specifically for nanoparticles with diameter larger than 25 nm, follows the exponential function in Equation (1) [18]:

$$\lambda_{abs} = \lambda_o + L_1 e^{L_2 d} \tag{1}$$

where λ_o, L_1, and L_2 are arbitrary constants of the exponential function and d is the diameter of the gold nanoparticles measured in nanometres. By fitting the graph, the values of λ_o, L_1, and L_2 are determined to be 512, 6.53 and 0.0216 respectively [18].

The diameter can be expressed in Equation (2) as follows;

$$d(nm) = \frac{1}{L_2}\left(\frac{\ln(\lambda_{abs} - \lambda_o)}{L_1}\right) \tag{2}$$

Based on Equation (2) and the wavelength of the absorbance peak shown in Fig. 1(a), the diameter of the gold nanoparticles was 62.2 nm, slightly smaller than the diameter obtained from the DLS analysis which measured a nominal diameter of 68.1 nm with a relatively narrow distribution as depicted in Fig. 1(b). The peak detected at sub-10 nm was also associated with the multiple scattering effects [20]. Equations (3) and (4) were applied to measure the concentration of the gold colloid. Assuming that the gold nanoparticles are spherical and have a face-centred cubic structure, the number of gold atoms per nanoparticle is calculated as follows:

$$n_{Au} = \frac{(\pi \rho_{Au} d^3)}{6 M_{Au}} \tag{3}$$

where ρ_{Au} and M_{Au} are the density and molecular weight of gold nanoparticles, respectively. Meanwhile, the number density of gold nanoparticles in the solution is expressed as:

$$C = \frac{N_{Au}}{n_{Au} \times N_A \times V} \tag{4}$$

where N_{Au} denotes the total number of gold atoms in the precursor solution, N_A is the Avogadro constant, and V represents the total volume of the solution.

The TEM image in Fig. 1(c) shows the morphology of the gold nanoparticles which are in spherical shapes while Fig. 1(d) depicts the size distribution of the gold nanoparticles that exhibits a nominal diameter of 44 nm and a standard deviation of 6.5 nm. The discrepancy of size measurements between the TEM and UV–vis absorbance and DLS could be due to the capping effect of the citrate layer on the gold

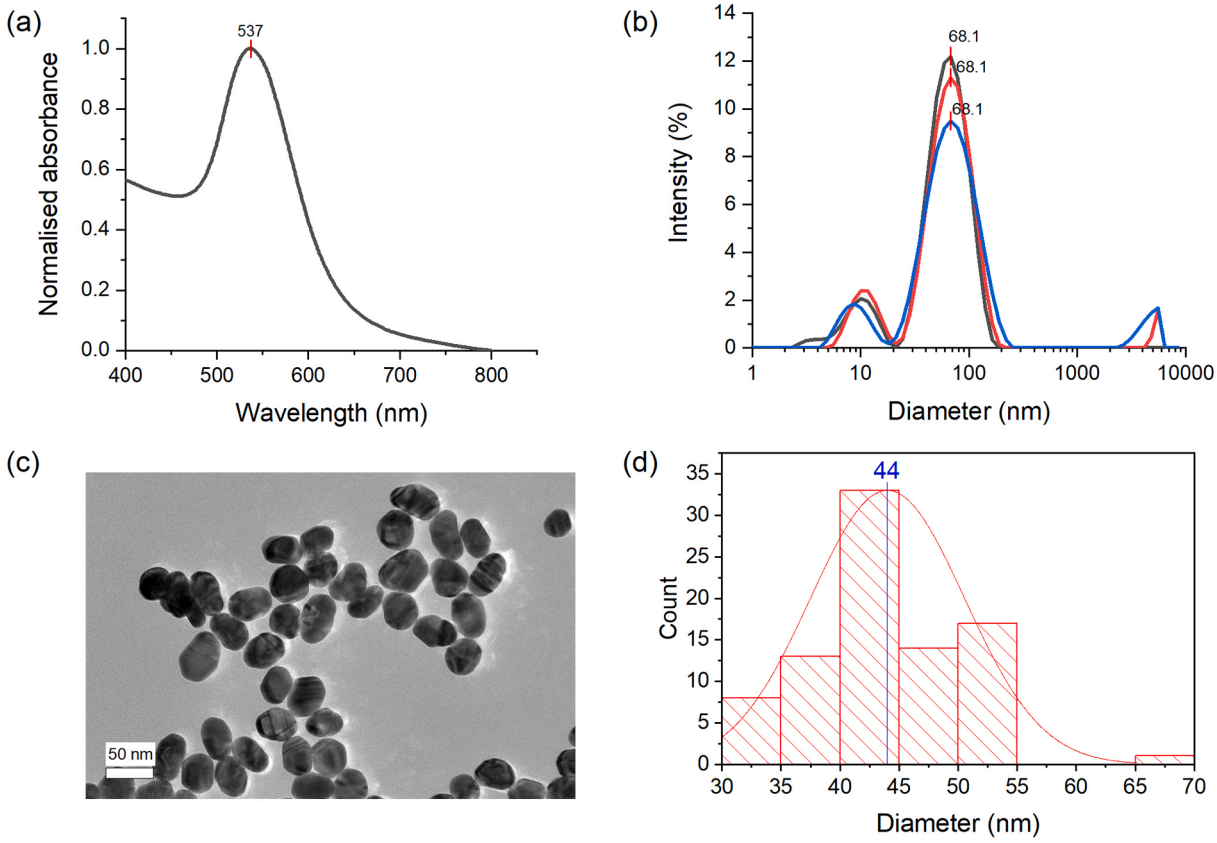

Fig. 1. Gold nanoparticles characterisations; (a) UV–vis absorbance spectrum, (b) size distribution obtained from the DLS analysis, (c) TEM image, and (d) size distribution attained from the TEM image. The scale bar in the TEM image represents 50 nm.

nanoparticles in DLS, which is highly sensitive to the gold nanoparticle ligands. Furthermore, Equations (3) and (4) and the nominal diameter of 44 nm were applied to estimate the colloid concentration, which was 5.72×10^{13} particles/mL. However, the particle density was 5.15×10^{15} particles/mL after being concentrated, assuming all nanoparticles were retained during centrifuging.

3.2. *Evaluation of Na_2SO_4 as the aggregating agent*

Citrate ions are typically weakly-bonded and negatively charged

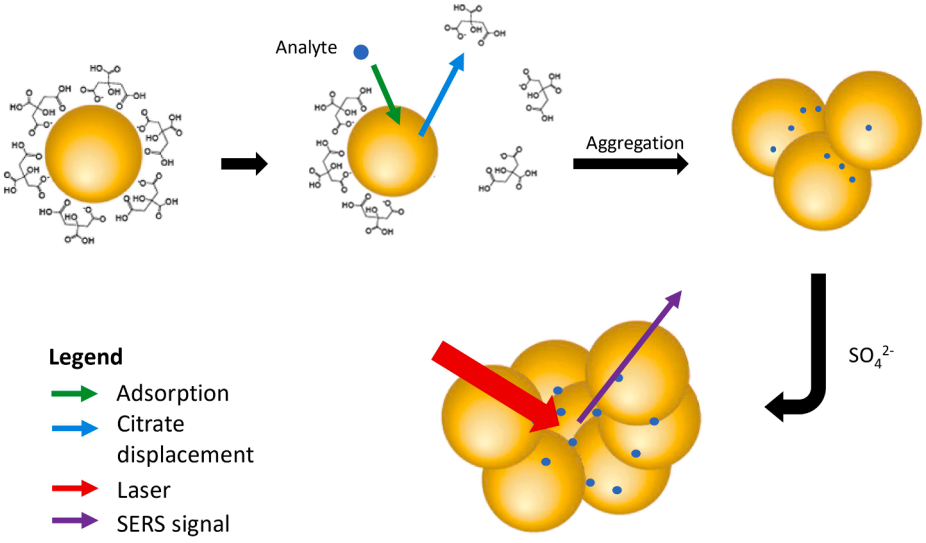

Fig. 2. The schematic of the interaction between analyte molecules and gold nanoparticles and the formation of aggregates in the presence of sulphate ion.

ligands. When added with analyte molecules, the citrate ions are displaced, and the analyte molecules are adsorbed onto the surface of the gold nanoparticles. The depleted surface charge results in a poor electromagnetic repulsion between the nanoparticles, leading to the formation of aggregates due to the influence of Van der Waals forces. The addition of sulphate ions (SO_4^{2-}) further reduces the surface of the nanoparticles, hence producing larger aggregates. The analyte molecules are entrapped in the nanogaps between the nanoparticles, generating the SERS hot spots, thus, highlighting of the interaction between analyte molecules, gold nanoparticles and SO_4^{2-} ions, as shown in Fig. 2.

The selection of aggregating agents is critical since certain ionic species exhibit a strong binding affinity to the nanoparticles and can block the analyte from adsorbing on the nanoparticle surface. For instance, the binding affinity of halide and SO_4^{2-} ions to gold nanoparticles are hypothetically similar to that of silver nanoparticles. Namely, halide ions possess a stronger bonding affinity to the surface of silver nanoparticles compared to SO_4^{2-} ions and can repel anionic analyte molecules from binding to the nanoparticle surface [6]. The acidity of the aggregating agents was adjusted to pH 3 to reduce the overall pH of the mixture. By assuming the gold nanoparticles and analyte mixture had a pH value of 7, the resulting pH of the mixture was 4.6. Lysozyme (isoelectric point at pH 11) has a positive charge at neutral pH while R6G recorded a stronger bonding to anionic gold nanoparticles [24]. Therefore, detecting R6G and lysozyme citrate capped gold nanoparticles were performed without any issue. Given that specific proteins exhibit isoelectric point lower than pH 7, it is necessary for a solution sample with complex matrices, such as grouper mucus, to become positively charged. The generation of the aggregates serves a vital role in forming the hot spots for the colloidal SERS. Ideally, small nanoclusters trap the analytes in the hot spots for the best SERS signal enhancement. In contrast, larger aggregates tend to shield the hot spots, decreasing the signal intensity [12]. Given that the initial aggregates formation significantly depends on the analyte, the effect of varying concentrations of the aggregating agent was explored with different analytes, which include lysozyme, R6G, and a complex matrix, grouper mucus.

The impact of adding Na_2SO_4 to the gold nanoparticles was assessed by comparing the SERS spectra of the mixture of gold nanoparticles and Na_2SO_4 solution without the presence of the analyte. In general, the gold nanoparticles contribute to a relatively blank background spectrum. A minor peak at 1537 cm^{-1} could be attributed to the asymmetric stretch of the citrate ligand's carboxylic (COO) group. The peak assignment for the citrate ligand on the gold nanoparticles surface is summarised in Table S1 of the supplementary material. The peak at 227 cm^{-1} is attributed to the Au-Cl bond [25]. The residual Cl^- ions from the gold (III) chloride ($HAuCl_4$) solution that was used in synthesising the gold nanoparticles, the peak was undetected in the non-aggregated gold nanoparticles. However, the peak appeared after adding the aggregating agent, which trapped the Cl^- ions in the SERS hot spots. Other peaks relating to the SO_4^{2-} ions were detected include 447 and 617 cm^{-1} (bending of SO_4^{2-}), 980 cm^{-1} (symmetric stretching) and 1100 cm^{-1} (anti-symmetric stretching) [26]. Remarkably, the SO_4^{2-} peaks were absent following the addition of Na_2SO_4 to the gold nanoparticles, as presented in Fig. 3. The Raman spectra remained relatively blank in this region, implying that the SO_4^{2-} ions were poorly adsorbed to the gold nanoparticle surface. Thus, Na_2SO_4 is considered a suitable aggregating agent, given its poor adsorption on the gold nanoparticle surface.

3.3. SERS of R6G using acidified Na_2SO_4 as the aggregating agent

In general, R6G is a fluorescent dye with characteristic Raman peaks in the region between 600 and 1700 cm^{-1}. Fig. 4(a) shows the effect of the aggregating agent on the SERS intensity of R6G was evaluated by adding acidified Na_2SO_4 solution at varying concentrations in the range of 0.1 and 2.0 M to the R6G and gold nanoparticles mixture. As shown in Fig. 4(b), adding gold nanoparticles greatly enhances the Raman peaks of R6G at a concentration of 0.1 mM, which were barely visible without gold nanoparticles.

Referring to Fig. 4(a), adding 0.1 M Na_2SO_4 initially decreased the signal intensity as the adsorbed R6G molecules were displaced from the gold nanoparticles' surface. The adsorbed R6G molecules can be displaced by mercury ions [27], thus, it can be inferred that the same phenomenon occurred with sulphate ions. However, beyond 0.1 M, the

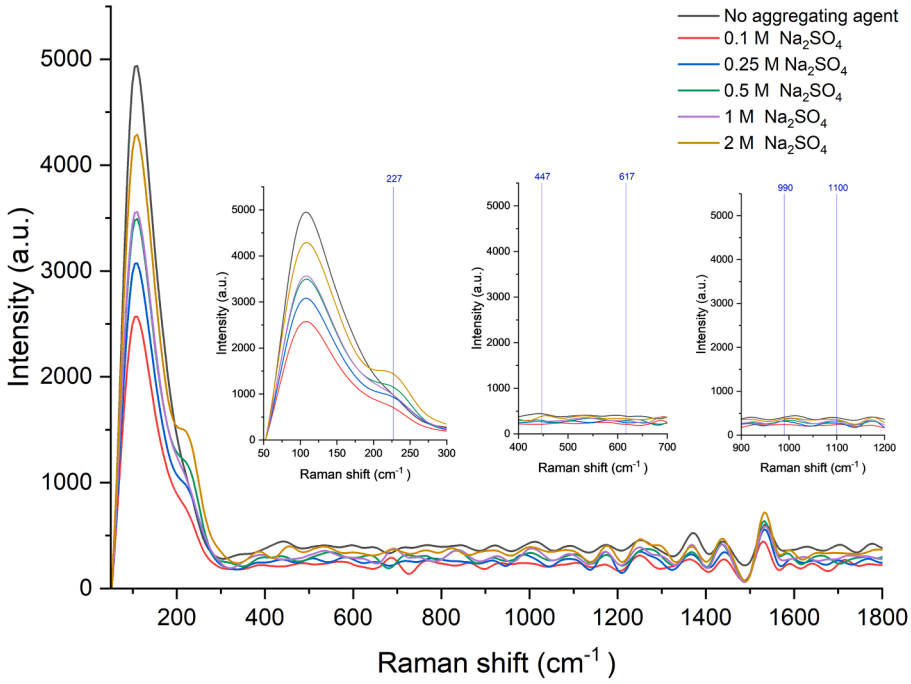

Fig. 3. SERS spectra of gold nanoparticles with different concentration of Na_2SO_4 without the presence of analyte. The insets show the region between 50 and 300 cm^{-1} (left), 400 to 700 cm^{-1} (centre) and 900 to 1100 cm^{-1} (right). The Au-Cl peak was located at 227 cm^{-1} while the SO_4^{2-} peaks were located at 447, 617, 980 and 1100 cm^{-1}.

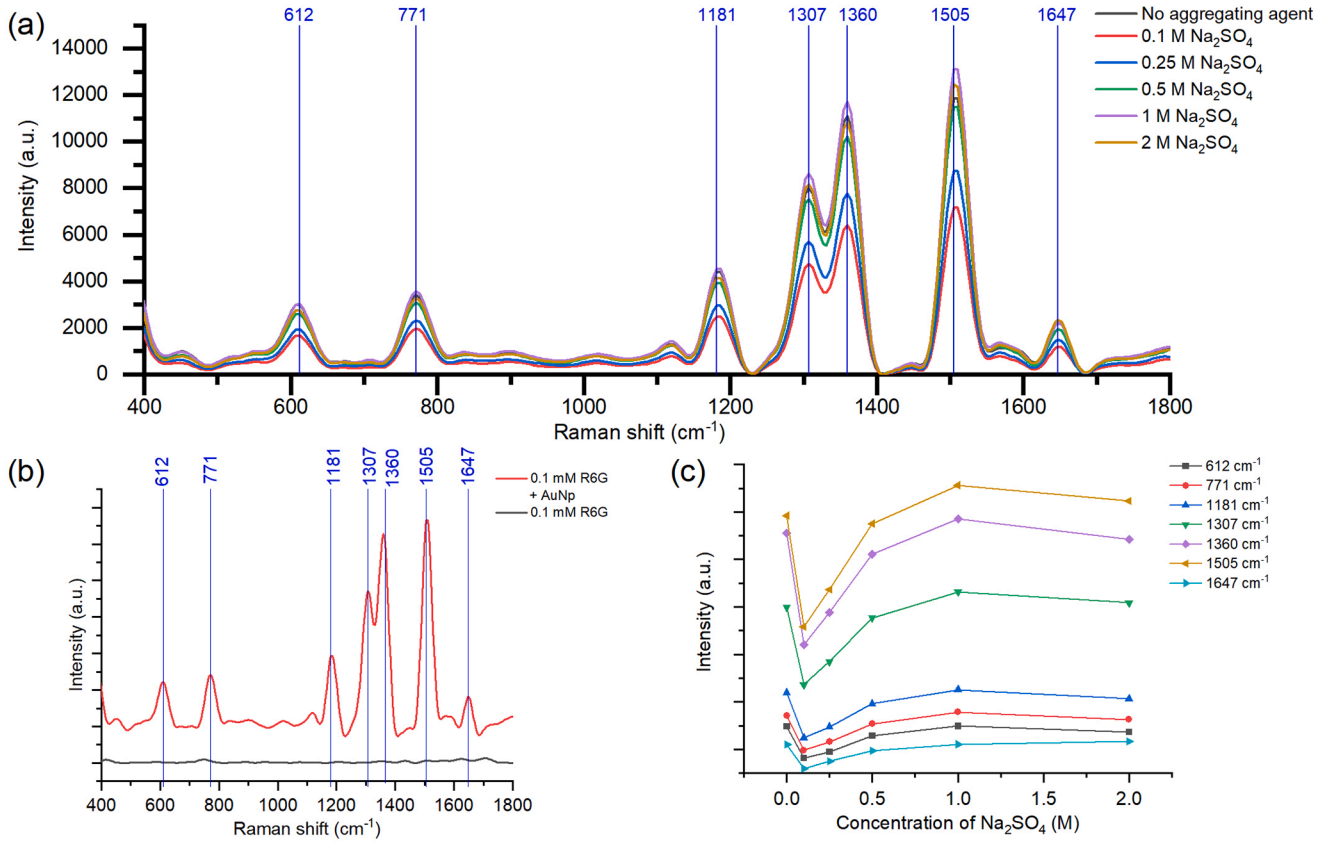

Fig. 4. (a) SERS spectra of R6G with addition different concentrations of acidified Na_2SO_4 as the aggregating agent. The significant peaks are labelled. (b) Raman spectra of 0.1 mM R6G with and without gold nanoparticles. The black line is the Raman spectrum of 0.1 mM R6G while the red line is the SERS spectrum of 0.1 mM R6G with the addition of gold nanoparticles. The spectra are shifted for clarity. Both spectra were acquired using 50 mW laser power and 10 s integration time. The intensity of the peaks labelled in (a) are plotted against the concentration of Na_2SO_4 in (c). The graphs in (c) represent the offset value for visual clarity. (For interpretation of the reference to colour in this figure legend, the reader is referred to the web version of this article.)

aggregate size increased with an increment concentration of Na_2SO_4. Fig. 4(c) shows the intensity of the peaks identified in Fig. 4(a) plotted against the concentration of Na_2SO_4 solution. The graphs were offset for visual clarity and to better observe the trend of the intensity of the peaks as the concentration of Na_2SO_4 increases. According to Fig. 4(c), adding 1 M Na_2SO_4 achieved an optimum degree of aggregation, which recorded the highest signal enhancement. Beyond 1 M concentration, the addition of the Na_2SO_4 formed larger aggregates that blocked the SERS hot spots, ultimately reducing the signal intensity. The peak assignment of R6G is listed in Table 1.

To discuss on the signal improvement by the colloidal gold, the enhancement factor (EF) is normally chosen as expressed in Equation (4):

$$EF = \frac{I_{SERS} C_{Raman}}{I_{Raman} C_{SERS}} \quad (4)$$

where I_{SERS} and C_{SERS} are the peak intensity obtained using SERS and the concentration of analyte molecules adsorbed on the surface of the gold nanoparticles, respectively. Meanwhile, I_{Raman} and C_{Raman} are the peak intensity obtained using Raman spectroscopy and the concentration of the analyte molecules exposed to the excitation laser beam, respectively. It is difficult to determine the exact region of the liquid droplet which is exposed to the laser beam [29]. However, since the ball lens was in contact with the liquid droplet during spectra acquisition, it could be reasonably assumed that the entire liquid droplet was exposed to the excitation laser. Using nominal diameter of 44 nm, and Equations (2) and (3), the concentration of gold nanoparticles is calculated to be 8.55 μM. Assuming that the number of R6G molecules adsorbed on the gold nanoparticles surface is equal to the number of gold nanoparticles present in the colloid, and using the intensities of the C–C bond peak located at 1505 cm^{-1} obtained using SERS and Raman spectroscopy in Fig. 4(b), the enhancement factor is estimated to be 1.027×10^4. Therefore, this result verifies that the synthesised gold nanoparticles are an effective colloidal SERS substrate.

Table 1
Peak assignment of R6G [28].

Peak centre (cm^{-1})	Peak assignment
606	C–C–C ring in plane vibration
711	C–H out of plane vibration
1181	C–H in plane vibration
1307	N–H in plane bend
1360	C–C stretching
1505	C–C stretching
1647	C–C stretching

3.4. SERS of lysozyme using acidified Na_2SO_4 as the aggregating agent

Fig. 5 depicts the experimental results and analyses using lysozyme as the target molecule in colloidal gold nanoparticles with acidified Na_2SO_4 as the aggregating agent. Proteins exhibit three characteristic vibrations resulting from the vibration of the polypeptide backbone. Specifically, the amide I band (1600 to 1700 cm^{-1}) is primarily associated with the C = O stretch of the amide carbonyl [30], while the amide III vibration (1200–1300 cm^{-1}) represents the out-of-phase combination of the N–H in-plane bend and C-N stretch with a minor contribution from the C=O in-plane bend and C–C stretch. Furthermore,

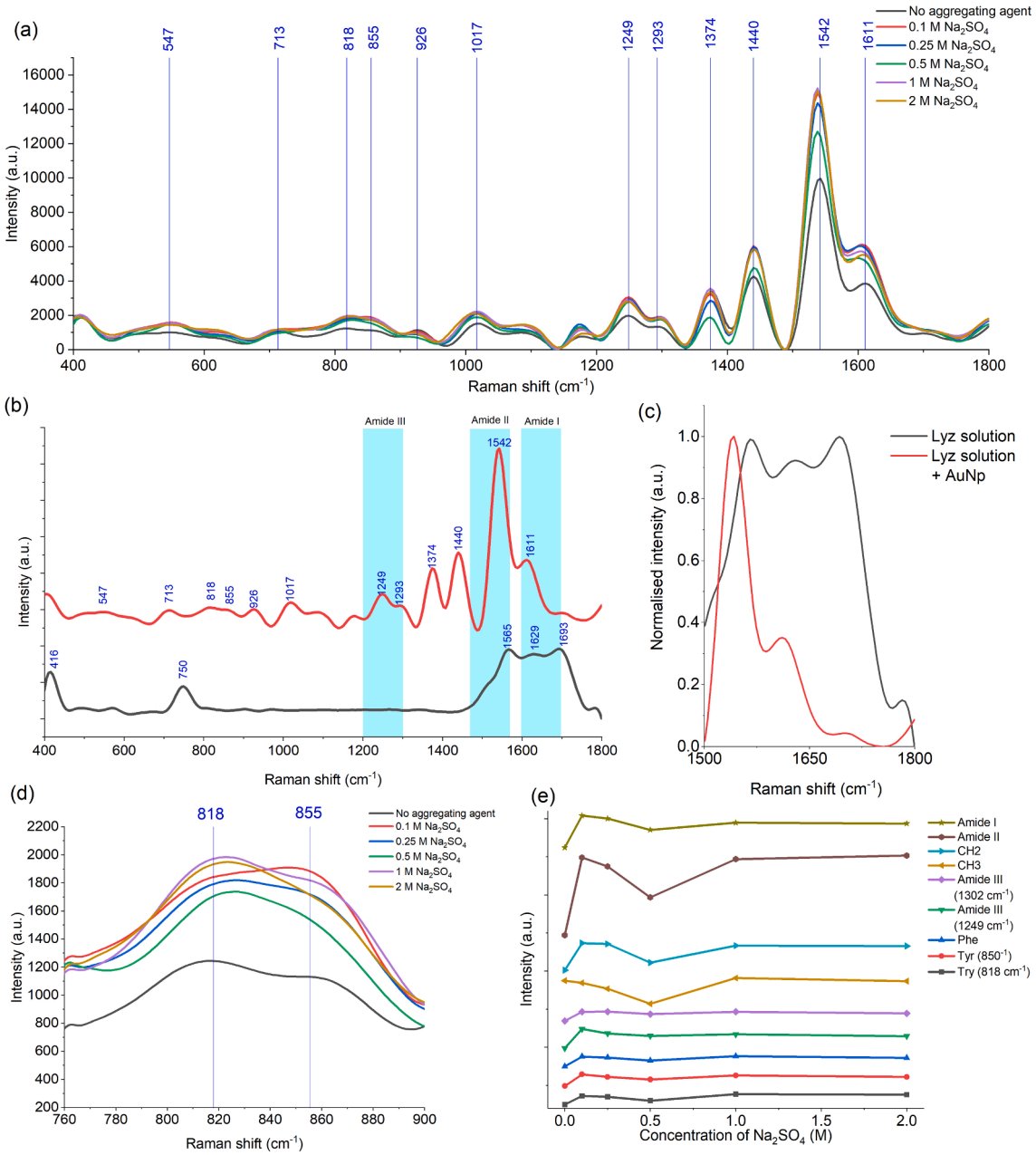

Fig. 5. (a) SERS spectra of 300 μg/mL lysozyme with the addition of different concentration of Na_2SO_4 as aggregating agent. (b) The Raman spectrum (black) and SERS spectrum (red) of lysozyme solution. Both spectra were obtained using 50 mW laser power and 10 s integration time. (c) The normalised Raman and SERS spectra of lysozyme in the region between 1500 and 1800 cm^{-1}. (d) The SERS spectra of lysozyme in the region between 760 and 900 cm^{-1}. The tyrosine doublet is labelled in the graph. The intensity of the peaks labelled in (a) plotted against the concentration of Na_2SO_4 in (e). The graphs in (e) represent the offset value for visual clarity. (For interpretation of the references to colour in this figure legend, the reader is referred to the web version of this article.)

the amide II (1480–1580 cm^{-1}) is the combination of N–H bend, C-N stretch and significant overlap with C–C stretch and C=O bend [31]. As depicted in Fig. 5(b), the lysozyme solution generates a relatively poor Raman spectrum, with the amide II at 1542 cm^{-1} as the most dominant band, while none of those from the amino acid side chains were detected. However, additional bands from the S-S and C-S stretch were also detected at 416 and 750 cm^{-1} respectively, indicating the presence of sulphur-containing amino acid residues and disulphide bonds, respectively.

Comparatively, the SERS spectrum of lysozyme with gold nanoparticles exhibits all the characteristic vibrations of the polypeptide backbone and the amino acid side chains as shown in Fig. 5(a). The peak assignment of the Raman and SERS spectra of lysozyme is summarised in Table 2. Considering instrumentation differences, the functional groups were assigned to within ± 10 cm^{-1} of the literature value [32,33,34].

The main difference between the Raman spectroscopy and SERS is the selection rules of the amide bands. In SERS, the large amino acid side chains block the peptide bond from the plasmonic nanostructures, suppressing the amide I vibration [35]. Thus, the signal intensity of the amide I band in the SERS spectrum was reduced, as viewed in Fig. 5(c), compared to the signal intensity of the lysozyme solution achieved in the Raman spectrum. Moreover, the blue-shifting of the amide I from the peak of 1629 to 1611 cm^{-1} suggests the structural conversion of the lysozyme from α-helical into β-sheets and random coil formation [36]. In addition, the tyrosine doublet was observed at 818 and 850 cm^{-1} which corresponds to the phenol ring breathing, and the Fermi resonance

between the phenol ring breathing and the out-of-plane mode of the phenol ring as shown in Fig. 5(d) [37]. As evident in Fig. 5(d), the ratio of the intensity of the peak at 818 and 855 cm^{-1} is low. This may be explained by the lack of π-π electrons interaction in liquid phase [37] or the nitration of the phenol ring in tyrosine due to the exposure of the laser light [38]. The higher degree of aggregation induced by lysozyme is also evident in Fig. 5(e), given that the highest signal enhancement was achieved at an optimal Na_2SO_4 concentration of 0.1 M. On the surface of the gold nanoparticles, lysozyme unfolds and forms protein-gold nanoparticles complexes that eventually coalesce to form aggregates [39]. Based on this finding, the optimal concentration value of Na_2SO_4 was much lower than the value of 1 M Na_2SO_4 for the optimal enhancement for R6G.

3.5. SERS of grouper mucus using acidified Na_2SO_4 as the aggregating agent

The complex matrix in grouper mucus comprises saccharides, lipids, proteins, and many other metabolites, as reflected in the SERS spectra. In this case, the SERS spectrum is the collective molecular vibrational mode of all the biomolecules in the mucus. The SERS spectra in Fig. 6(a) show the significant peaks of the grouper mucus, while Table 3 summarises the corresponding tentative peak assignments within ± 10 cm^{-1} of the literature values [32,33,34] to account for the instrumental differences. The characteristic tyrosine doublet was observed in Fig. 6(a), however, similar to the case observed in the SERS spectra of lysozyme in Fig. 5(d), the shape of the tyrosine doublet observed in the SERS spectra of grouper epidermal mucus may be due to the lower interaction between the phenol ring in aqueous state [37] or nitration of the tyrosine induced by the laser light [38]. Although Fig. 6(b) shows that an optimal concentration of 1 M recorded the most enhanced SERS signal of grouper mucus, the signal intensity was inconsistent between peaks. As such, increasing the size of the aggregating agent beyond 0.1 M reduced the peak intensity at 839 cm^{-1}, which corresponds to tyrosine residues. Similarly, the addition of the aggregating agent decreased the peak intensity at 542 cm^{-1}, which is linked to the disulphide bridge.

Comparatively, the peaks corresponding to the polypeptide backbone showed the highest enhancement at 1 M. In contrast, the peak at 997 cm^{-1}, which refers to the phenylalanine residue and aromatic rings, recorded a higher maximum enhancement at 2 M. Following the addition of 0.1 M Na_2SO_4, the analyte molecules were displaced from the surface of the gold nanoparticles in the presence of SO_4^{2-} ions. Considering lysozyme as a critical immune constituent in fish epidermal mucus [2], the normalised SERS spectra of lysozyme were compared to those of grouper mucus, as presented in Fig. 6(c). The spectra were normalised using standard normal variate.

Table 2
Peak assignment of lysozyme.

Peak (cm^{-1})	Raman	SERS	Peak assignment
406		✓	S-S stretch
416	✓		
713		✓	C-S stretch (aliphatic)
750	✓		
818		✓	Tyr
850		✓	
926		✓	C–C-N deformation
1017		✓	Phe
1249		✓	Amide III
1293		✓	
1374		✓	CH_3 deformation
1440		✓	CH_2 deformation
1542		✓	Trp, amide II
1565	✓		Amide II
1611		✓	Amide I
1629	✓		
1693	✓		

Based on the results, overlapping peaks were located at 818, 859, 1283, 1454 and 1542 cm^{-1} corresponding to tyrosine residues, amide III, CH_2 and CH_3 stretch and, amide II, respectively. The observation of the characteristic tyrosine doublet in Fig. 6(c) confirms the presence of tyrosine [38]. However, the peak at 1454 cm^{-1} may not necessarily imply the presence of lysozyme in the grouper mucus since CH_2 and CH_3 bonds are typically found in various biomolecules. Furthermore, the amide III envelope in the 1200–1300 cm^{-1} range of lysozyme significantly differed from that of grouper mucus, signifying the multiplexing of numerous proteins and other biomolecules. Apart from that, the peak position of the tyrosine residue and amide II peak were similar. Overall, this study demonstrates a preliminary outlook at the possible detection of lysozyme in grouper mucus using SERS. Nevertheless, using the SERS spectra solely to characterise the biomolecules in the grouper mucus is challenging without supporting analysis from proteomics and metabolomics studies [3].

4. Conclusion and recommendations

This work demonstrates the potential of SERS technique in identifying grouper epidermal mucus using acidified Na_2SO_4 solution as an aggregating agent. This research work assessed the association between the concentration of the acidified Na_2SO_4 solution and the SERS intensity of various analytes. The ideal Na_2SO_4 concentration of 1.0 and 0.1 M recorded the highest signal enhancement for 1 mM R6G dye and 300 μg/mL lysozyme, respectively. A lower concentration of Na_2SO_4 was sufficient to achieve the highest signal enhancement for the lysozyme solution, given the strong influence of lysozyme on the gold nanoparticle aggregation. Although Na_2SO_4 also recorded an optimal concentration of 1 M for the SERS of grouper mucus, the results were inconsistent across all peaks, with only the peaks corresponding to proteins showing the highest enhancement. The few overlapping peaks of the SERS spectra of lysozyme and grouper mucus open up the potential for SERS-based analysis of grouper epidermal mucus for fish health using advanced data analysis.

Availability of data and material

The raw spectral data and pre-processed spectral data are available upon request.

Ethics approval

This study used hybrid groupers (*Epinephelus fuscoguttatus* × *Epinephelus lanceolatus*). Prior to the experimentation, the proposal for this study was reviewed and approved by the Institutional Animal Care and Use Committee, Universiti Putra Malaysia (UPM/ACUC/AUP-R054/2022).

Funding

This research work is fully funded by the Ministry of Higher Education, Malaysia under the Transdisciplinary Research Grant Scheme (TRGS/1/2020/UPM/02/1/1).

CRediT authorship contribution statement

Nathaniel Leong: Formal analysis, Investigation, Visualization, Writing – original draft, Writing – review & editing. **Mohd Hanif Yaacob:** Methodology, Supervision. **Ahmad Rifqi Md Zain:** Methodology, Supervision. **Tengku Hasnan Tengku Abdul Aziz:** Methodology, Supervision. **Annie Christianus:** Resources, Supervision. **Chou Min Chong:** Resources, Supervision. **Mohd Adzir Mahdi:** Funding acquisition, Project administration, Supervision, Writing – review & editing.

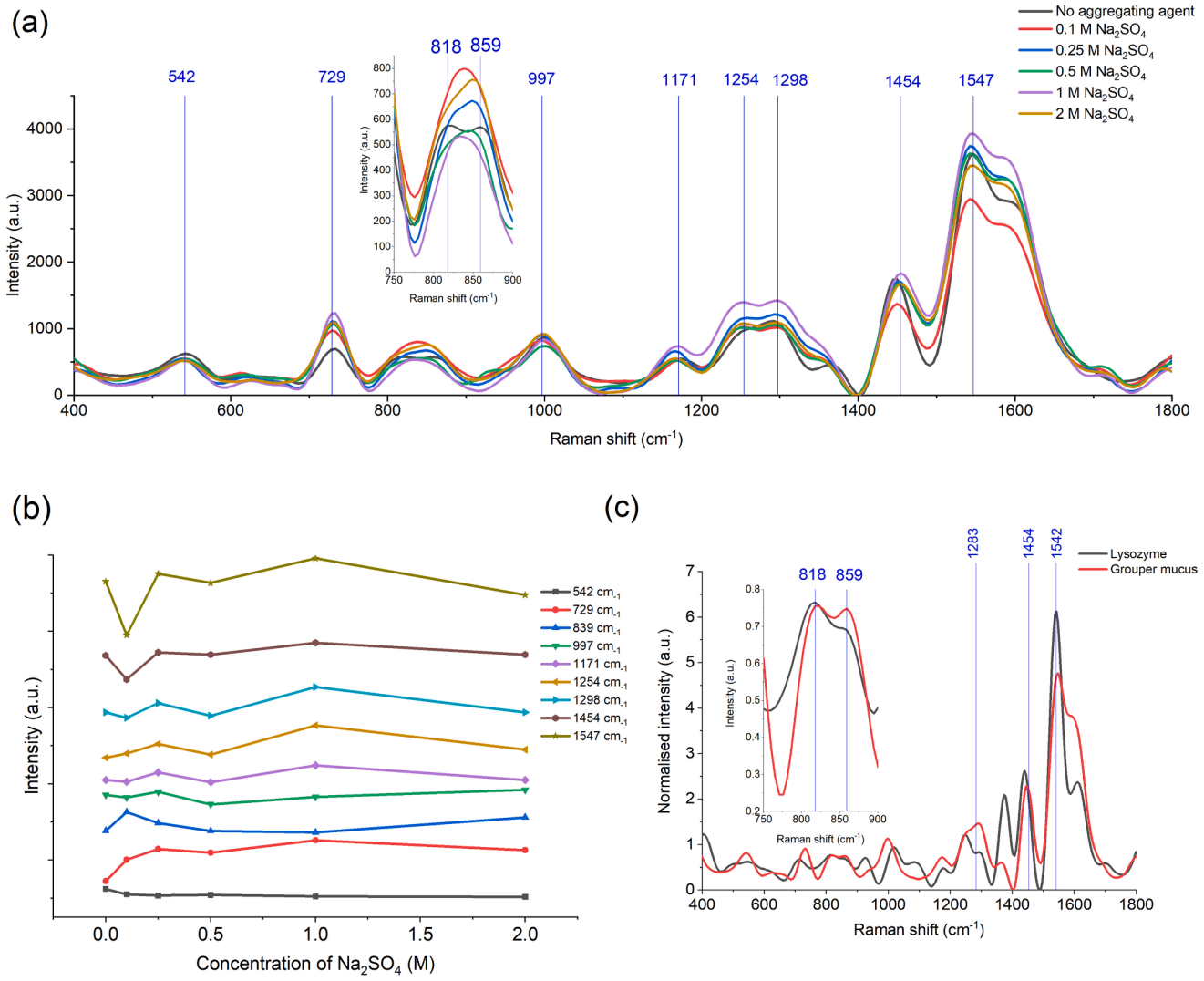

Fig. 6. (a) SERS spectra of grouper mucus with the addition of different concentration of Na_2SO_4. The inset shows the region between 750 and 900 cm^{-1} with the tyrosine doublet labelled. (b) The intensity of the peaks in (a) plotted against different concentration of Na_2SO_4. The graphs in (b) were shifted for clarity and the y-axis does not represent absolute intensity. (c) The normalised SERS spectra of lysozyme and grouper mucus. The inset shows the region between 750 and 900 cm^{-1} with the tyrosine doublet labelled.

Table 3
Tentative peak assignment of grouper mucus.

Peak (cm^{-1})	Tentative peak assignment
542	S-S stretch
729	C-S stretch
818	Tyr, C-O-C
850	
997	Phe, aromatic ring
1171	Tyr, C-N stretch
1254	Amide III
1298	
1454	CH_2 stretch, CH_3 stretch
1547	Amide II

Declaration of competing interest

The authors declare that they have no known competing financial interests or personal relationships that could have appeared to influence the work reported in this paper.

Data availability

Data will be made available on request.

Appendix A. Supplementary data

Supplementary data to this article can be found online at https://doi.org/10.1016/j.saa.2024.123974.

References

[1] G. Zaccone, B.G. Kapoor, S. Fasulo, L. Ainis, Structural, histochemical and functional aspects of the epidermis of fishes, in: Advances in Marine Biology, vol. 40, Academic Press, United States, 2001, pp. 253–348, https://doi.org/10.1016/S0065-2881(01)40004-6.
[2] S. Dash, S.K. Das, J. Samal, H.N. Thatoi, Epidermal mucus, a major determinant in fish health: A review, Iranian J. Veterinary Res. 19 (2) (2018) 72–81, https://doi.org/10.22099/ijvr.2018.4849.
[3] M.E. Natnan, C.F. Low, C.M. Chong, H. Bunawan, S.N. Baharum, Integration of omics tools for understanding the fish immune response due to microbial challenge, Front. Marine Sci. 8 (June) (2021), https://doi.org/10.3389/fmars.2021.668771.
[4] W.E. Smith, Practical understanding and use of surface enhanced Raman scattering/surface enhanced resonance Raman scattering in chemical and

biological analysis, Chem. Soc. Rev. 37 (5) (2008) 955–964, https://doi.org/10.1039/B708841H.
[5] L.E. Jamieson, S.M. Asiala, K. Gracie, K. Faulds, D. Graham, Bioanalytical measurements enabled by surface-enhanced Raman scattering (SERS) probes, Annu. Rev. Anal. Chem. 10 (Jul. 2017) 54.
[6] X.X. Han, G.G. Huang, B. Zhao, Y. Ozaki, Label-free highly sensitive detection of proteins in aqueous solutions using surface-enhanced Raman scattering, Anal. Chem. 81 (9) (May 2009) 3329–3333, https://doi.org/10.1021/ac900395x.
[7] X. Li, T. Yang, S. Li, D. Wang, Y. Song, K. Yu, Different classification algorithms and serum surface enhanced Raman spectroscopy for noninvasive discrimination of gastric diseases, J. Raman Spectrosc. 47 (8) (Aug. 2016) 917–925, https://doi.org/10.1002/jrs.4924.
[8] A. Stefancu, et al., SERS-based liquid biopsy of saliva and serum from patients with Sjögren's syndrome, Anal. Bioanal. Chem. 411 (22) (2019) 5877–5883, https://doi.org/10.1007/s00216-019-01969-x.
[9] G.D. Mistro, et al., Surface–enhanced raman spectroscopy of urine for prostate cancer detection: A preliminary study, Anal. Bioanal. Chem. 407 (12) (2015) 3271–3275, https://doi.org/10.1007/s00216-015-8610-9.
[10] C.D. Bocsa, V. Moisoiu, A. Stefancu, L.F. Leopold, N. Leopold, D. Fodor, Knee osteoarthritis grading by resonant Raman and surface-enhanced Raman scattering (SERS) analysis of synovial fluid, Nanomed.: Nanotechnol. Biol. Med. 20 (2019) 102012, https://doi.org/10.1016/j.nano.2019.04.015.
[11] L. Xue, B. Yan, Y. Li, Y. Tan, X. Luo, M. Wang, Surface-enhanced raman spectroscopy of blood serum based on gold nanoparticles for tumor stages detection and histologic grades classification of oral squamous cell carcinoma, Int. J. Nanomed. 13 (2018) 4977–4986, https://doi.org/10.2147/IJN.S167996.
[12] V. Turzhitsky, et al., Picoanalysis of drugs in biofluids with quantitative label-free surface-enhanced Raman spectroscopy, Small 14 (47) (2018) 1–11, https://doi.org/10.1002/smll.201802392.
[13] G. Das, et al., Nano-patterned SERS substrate: Application for protein analysis vs. temperature, Biosens. Bioelectron. 24 (6) (Feb. 2009) 1693–1699, https://doi.org/10.1016/j.bios.2008.08.050.
[14] C. Zhang, S. Chen, Z. Jiang, Z. Shi, J. Wang, L. Du, Highly sensitive and reproducible SERS substrates based on ordered micropyramid array and silver nanoparticles, ACS Appl. Mater. Interfaces 13 (24) (Jun. 2021) 29222–29229, https://doi.org/10.1021/acsami.1c08712.
[15] S.D. Iancu, et al., SERS liquid biopsy in breast cancer. What can we learn from SERS on serum and urine? Spectrochim. Acta Part A: Mol. Biomol. Spectroscopy 273 (May 2022) 120992 https://doi.org/10.1016/j.saa.2022.120992.
[16] A. Subaihi, et al., Rapid, accurate, and quantitative detection of propranolol in multiple human biofluids via surface-enhanced Raman scattering, Anal. Chem. 88 (22) (Nov. 2016) 10884–10892, https://doi.org/10.1021/acs.analchem.6b02041.
[17] J. Turkevich, P.C. Stevenson, J. Hillier, A study of the nucleation and growth processes in the synthesis of colloidal gold, Discuss. Faraday Soc. 11 (1951) 55–75, https://doi.org/10.1039/DF9511100055.
[18] W. Haiss, N.T.K. Thanh, J. Aveyard, D.G. Fernig, Determination of size and concentration of gold nanoparticles from UV−vis spectra, Anal. Chem. 79 (11) (Jun. 2007) 4215–4221, https://doi.org/10.1021/ac0702084.
[19] A.E. Vladár, V.-D. Hodoroaba, Chapter 2.1.1 - Characterization of nanoparticles by scanning electron microscopy, in: V.-D. Hodoroaba, W.E.S. Unger, A.G. Shard (Eds.), Characterization of Nanoparticles, Elsevier, 2020, pp. 7–27, https://doi.org/10.1016/B978-0-12-814182-3.00002-X.
[20] T. Zheng, S. Bott, Q. Huo, Techniques for accurate sizing of gold nanoparticles using dynamic light scattering with particular application to chemical and biological sensing based on aggregate formation, ACS Appl. Mater. Interfaces 8 (33) (Aug. 2016) 21585–21594, https://doi.org/10.1021/acsami.6b06903.
[21] M. Rożyński, M. Hopko, K. Stawecki, Z. Zakęś, Impact of fish size, water temperature, and MS-222 concentration on inducing general anesthesia in pikeperch (sander lucioperca), Aquac. Res. 49 (8) (Aug. 2018) 2774–2781, https://doi.org/10.1111/are.13738.
[22] R. Tantra, R.J.C. Brown, M.J.T. Milton, Strategy to improve the reproducibility of colloidal SERS, J. Raman Spectrosc. 38 (11) (Nov. 2007) 1469–1479, https://doi.org/10.1002/jrs.1797.
[23] A. R. M. Radzol, K. Y. Lee, W. Mansor, A. Azman, "Optimization of Savitzky-Golay smoothing filter for salivary surface enhanced Raman spectra of non structural protein 1," presented at the TENCON 2014 - 2014 IEEE Region 10 Conference, 2014, pp. 1–6. doi: 10.1109/TENCON.2014.7022409.
[24] E.-O. Ganbold, J.-H. Park, U. Dembereldorj, K.-S. Ock, S.-W. Joo, Charge-dependent adsorption of rhodamine 6G on gold nanoparticle surfaces: fluorescence and Raman study, J. Raman Spectrosc. 42 (8) (Aug. 2011) 1614–1619, https://doi.org/10.1002/jrs.2907.
[25] X. Liu, et al., Sub-angstrom gold nanoparticle/liposome interfaces controlled by halides, Langmuir 34 (22) (2018) 6628–6635, https://doi.org/10.1021/acs.langmuir.8b01138.
[26] I. Lee, et al., Raman-spectroscopic investigation of sulfate ion concentration change in a continuously stirred tank reactor during the preparation of a cathode material precursor, Electrochim. Acta 246 (2017) 864–869, https://doi.org/10.1016/j.electacta.2017.06.107.
[27] H.-Y. Chang, T.-M. Hsiung, Y.-F. Huang, C.-C. Huang, Using rhodamine 6G-modified gold nanoparticles to detect organic mercury species in highly saline solutions, Environ. Sci. Tech. 45 (4) (Feb. 2011) 1534–1539, https://doi.org/10.1021/es103369d.
[28] C. Wu, E. Chen, J. Wei, Surface enhanced Raman spectroscopy of Rhodamine 6G on agglomerates of different-sized silver truncated nanotriangles, Colloids Surf A Physicochem Eng Asp 506 (2016) 450–456, https://doi.org/10.1016/j.colsurfa.2016.07.020.
[29] M.V. Cañamares, J.V. Garcia-Ramos, S. Sanchez-Cortes, M. Castillejo, M. Oujja, Comparative SERS effectiveness of silver nanoparticles prepared by different methods: A study of the enhancement factor and the interfacial properties, J. Colloid Interface Sci. 326 (1) (Oct. 2008) 103–109, https://doi.org/10.1016/j.jcis.2008.06.052.
[30] A. Sadat, I.J. Joye, Peak fitting applied to Fourier transform infrared and Raman spectroscopic analysis of proteins, Appl. Sci. (Switzerland) 10 (17) (2020), https://doi.org/10.3390/app10175918.
[31] S. Krimm, J. Bandekar, Vibrational spectroscopy and conformation of peptides, polypeptides, and proteins, in: C.B. Anfinsen, J.T. Edsall, F.M.B.T.-A.P.C. Richards (Eds.), vol. 38, Academic Press, United States, 1986, pp. 181–364. doi: 10.1016/S0065-3233(08)60528-8.
[32] A. Rygula, K. Majzner, K.M. Marzec, A. Kaczor, M. Pilarczyk, M. Baranska, Raman spectroscopy of proteins: A review, J. Raman Spectrosc. 44 (8) (2013) 1061–1076, https://doi.org/10.1002/jrs.4335.
[33] G.P. Szekeres, J. Kneipp, SERS probing of proteins in gold nanoparticle agglomerates, Front. Chem. 7 (JAN) (2019) 1–10, https://doi.org/10.3389/fchem.2019.00030.
[34] Horiba Jobin Yvon, Raman Spectroscopy for Analysis and Monitoring, *Horiba Jobin Yvon, Raman Application Note*, 2017, pp. 1–2.
[35] D. Kurouski, T. Postiglione, T. Deckert-Gaudig, V. Deckert, I.K. Lednev, Amide I vibrational mode suppression in surface (SERS) and tip (TERS) enhanced Raman spectra of protein specimens, Analyst 138 (6) (2013) 1665–1673, https://doi.org/10.1039/C2AN36478F.
[36] A. Sethuraman, G. Belfort, Protein structural perturbation and aggregation on homogeneous surfaces, Biophys. J . 88 (2) (Feb. 2005) 1322–1333, https://doi.org/10.1529/biophysj.104.051797.
[37] B. Hernández, Y.-M. Coïc, F. Pflüger, S.G. Kruglik, M. Ghomi, All characteristic Raman markers of tyrosine and tyrosinate originate from phenol ring fundamental vibrations, J. Raman Spectrosc. 47 (2) (Feb. 2016) 210–220, https://doi.org/10.1002/jrs.4776.
[38] P. Niederhafner, M. Šafařík, J. Neburková, T.A. Keiderling, P. Bouř, J. Šebestík, Monitoring peptide tyrosine nitration by spectroscopic methods, Amino Acids 53 (4) (Apr. 2021) 517–532, https://doi.org/10.1007/s00726-020-02911-7.
[39] D. Zhang, et al., Gold nanoparticles can induce the formation of protein-based aggregates at physiological pH, Nano Lett. 9 (2) (2009) 666–671, https://doi.org/10.1021/n1803054h.